

## ARTICLE OPEN



# Serious underestimation of reduced carbon uptake due to vegetation compound droughts

Jiayi Song<sup>1,2</sup>, Sha Zhou<sup>1,2</sup>✉, Bofu Yu<sup>3</sup>, Yan Li<sup>1,2</sup>, Yanxu Liu<sup>1,2</sup>, Ying Yao<sup>1,2</sup>, Shuai Wang<sup>1,2</sup> and Bojie Fu<sup>1,2,4</sup>

Compound droughts with low soil moisture (SM) and high vapor pressure deficit (VPD) pose significant threats to terrestrial carbon sink and agricultural production. However, the frequency and intensity of compound droughts and their adverse impacts on the carbon cycle remain highly uncertain. Here, we define and identify vegetation compound droughts (VCDs) when low SM and high VPD severely limit and adversely affect vegetation carbon uptake. We find frequent and severe VCDs and their considerable adverse impacts on carbon uptake in mid- and low-latitude regions, particularly in drylands. Risks of VCDs have been greatly underestimated as the widely adopted quantile-based approach identifies only 11% of VCDs and 26% of global GPP anomalies due to VCDs. The frequency and intensity of VCDs and their adverse impacts on carbon uptake are projected to increase further, irrespective of whether the CO<sub>2</sub> fertilization effect on vegetation growth and photosynthesis is considered or not. These findings improve our understanding of current and future risks of VCDs and underline the importance of adaptation measures to cope with the adverse impacts of ever-increasing compound droughts.

*npj Climate and Atmospheric Science* (2024)7:23; <https://doi.org/10.1038/s41612-024-00571-y>

## INTRODUCTION

Anthropogenic climate change increases the frequency, intensity, and severity of climate extremes such as droughts and heatwaves<sup>1–3</sup>, which threaten ecological and societal sustainability<sup>4,5</sup>. Drought directly limits terrestrial water availability and carbon uptake through low soil moisture (SM) and/or high vapor pressure deficit (VPD)<sup>6,7</sup>, and extreme water stress can substantially reduce agricultural production<sup>8,9</sup> and bring about widespread vegetation mortality<sup>10,11</sup>. Specifically, drought suppresses photosynthetic assimilation rates by reducing stomatal conductance and related enzyme activity<sup>6,12</sup> and inducing leaf senescence and abscission as well<sup>13</sup>, resulting in reduced gross primary productivity (GPP) at the ecosystem scale. When water is limited, compound droughts (CDs) characterized by concurrent low SM and high VPD would cause even greater reductions in GPP than soil drought (low SM) or atmospheric aridity (high VPD) alone<sup>14,15</sup>. Low SM and high VPD tend to occur simultaneously over much of the global land surface, as SM deficits reduce evapotranspiration and increase sensible heat flux, resulting in a drier and warmer atmosphere and a higher VPD, and the high VPD in turn enhances evaporative water loss and accelerates reduction in SM<sup>16,17</sup>. CDs are projected to become more frequent and more extreme, which could greatly reduce land carbon sink and compromise climate mitigation efforts<sup>3,14</sup>. However, assessments of past and future changes in CDs largely focus on extreme events from a statistical perspective<sup>4,17,18</sup> without taking into account whether these events cause adverse impacts on the environment. As there is not yet a general consensus on the definition of compound events, global assessment of CDs and their impacts on terrestrial ecosystem productivity are varied and uncertain<sup>4,14,19,20</sup>. An improved understanding and accurate assessment of global CDs and particularly their impacts on terrestrial carbon uptake are

therefore crucial for better management and mitigation of the ever-increasing drought risks in a warmer world.

Compound events have been typically defined as events when multiple dependent variables exceed extreme quantile-based thresholds<sup>4,5,14,17,18</sup>. However, from an impact-centric perspective, drivers of a compound event do not need to be extreme individually in a statistical sense, but the co-occurrence of these drivers at the same location could lead to an amplified societal or environmental impact<sup>19,20</sup>. Indeed, adverse impacts can occur even if not all relevant variables are extreme, and the predefined extreme quantile does not necessarily cause adverse impacts under certain circumstances. For example, when CDs are defined as months with SM below its 10th percentile and VPD above its 90th percentile, this definition has been shown to be problematic for high-latitude regions where vegetation production in fact increases with air temperature and VPD as bioproduction is not limited by water availability<sup>14</sup>. On the other hand, a quantile-based definition may also underestimate the frequency of occurrence of CDs and their adverse impacts on terrestrial carbon uptake in drylands. Although plants in drylands can maintain photosynthesis with limited water supply through their morphology and physiology<sup>21–23</sup>, ecosystem productivity is predominantly controlled by water availability<sup>24,25</sup>. Frequent and severe droughts directly reduce carbon uptake in drylands, and dryland ecosystems contribute a large proportion to the interannual variability of global terrestrial carbon sink<sup>26,27</sup>. Such uncertainty associated with the quantile-based definition hinders our understanding of the current and future risks of CDs, undermines reliable projection of terrestrial carbon sink, and calls for a more suitable definition of CDs from an impact-centric perspective.

In this study, we propose a framework to define CDs based on how the GPP responds to low SM and high VPD and provide an improved assessment of the frequency, intensity, and severity of

<sup>1</sup>State Key Laboratory of Earth Surface Processes and Resource Ecology, Faculty of Geographical Science, Beijing Normal University, Beijing, China. <sup>2</sup>Institute of Land Surface System and Sustainable Development, Faculty of Geographical Science, Beijing Normal University, Beijing, China. <sup>3</sup>School of Engineering and Built Environment, Griffith University, Nathan, Queensland, Australia. <sup>4</sup>State Key Laboratory of Urban and Regional Ecology, Research Center for Eco-Environmental Sciences, Chinese Academy of Sciences, Beijing, China. ✉email: shazhou21@bnu.edu.cn

CDs and associated impacts on terrestrial carbon uptake over past decades and in the future with a warmer climate. In this framework, we identify soil droughts and atmospheric aridity based on the assumption that low SM and high VPD strongly limit GPP, i.e., GPP increases with SM and decreases with VPD under water-limited conditions, and together they cause adverse impacts on GPP. CDs are identified when soil droughts and atmospheric aridity occur simultaneously during the warm season (see “Methods”). This impact-based approach is applied to identification of CDs and associated impacts on terrestrial carbon uptake at the monthly scale using observations (SM from GLEAM dataset v3.5a, VPD from MERRA-2 reanalysis, and GPP from FLUXCOM products)<sup>28–30</sup> for the period of 1981–2017 and historical (1930–2014) and future (2016–2100) simulations under the low (shared socioeconomic pathways SSP1-2.6) and high (SSP5-8.5) emission scenarios from Coupled Model Intercomparison Project Phase6 (CMIP6).

## RESULTS

### Identification and characteristics of compound droughts

Many observational and modeling studies show that GPP responds to SM and VPD in a highly non-monotonic manner<sup>7,14,31–36</sup> (Supplementary Fig. 1). SM directly determines the amount of water that can be used for vegetation growth and primary production, and GPP always increases with SM when water is limited, while excessive SM associated with high rainfall may cause GPP to decrease<sup>7,34,35</sup>. On the other hand, in an environment with low temperature and low VPD, an increase in VPD promotes GPP as warming enhances photosynthetic activity and vegetation growth, but extreme high VPD may induce closure of plant stomata to minimize water loss through transpiration, which inhibits plant photosynthesis and GPP decreases<sup>6,14,32</sup>. Given the non-monotonic response of GPP to SM and VPD, we identify the SM and VPD thresholds that severely limit and exert negative impacts on GPP using the segmented linear regression to quantify the relationship between GPP and SM or VPD for each grid cell (see “Methods”). The change-point of SM above which GPP no longer increases with SM in the segmented regression is compared with the SM associated with zero GPP anomaly, and the threshold is identified as the lower of the two SM values so that soil droughts occur when the SM falls below the threshold with negative GPP anomalies (Fig. 1e). Similarly, the threshold of VPD is identified as the higher of two VPD values of the change-point VPD and the VPD associated with zero GPP anomaly (Fig. 1f). CDs are therefore defined as months in the warm season when SM falls below the SM threshold and VPD exceeds the VPD threshold simultaneously. CDs identified with this impact-based definition, henceforth called vegetation compound droughts (VCDs), are compared with those defined with the quantile-based definition, i.e., months when SM falls below its 10th percentile and at the same time VPD exceeds its 90th percentile for that month<sup>14</sup>. The latter is henceforth called statistical compound droughts (SCDs).

To evaluate the effectiveness of the impact-based definition, we first assess the average GPP anomalies when VCDs occur using observational products and CMIP6 historical simulations. VCDs are detected over 66% of the land area (excluding Antarctica and Greenland) based on observations and over 91% of the land area in CMIP6 simulations, with 61% of the land area detected in at least 50% models (Fig. 1a, c). Over these areas, we find negative GPP anomalies for soil droughts (months when SM falls below its threshold), atmospheric aridity (months when VPD exceeds its threshold), and hence VCDs (Fig. 1a, c and Supplementary Fig. 2). It is worth noting that atmospheric aridity and VCDs are not detected in many high-latitude regions where vegetation growth and carbon uptake are essentially temperature-limited and GPP always increases with VPD (Fig. 1a, c and Supplementary Fig. 2).

The global patterns of average GPP anomalies for VCDs are broadly consistent between observations and models ( $r = 0.54$ ), with the global area-weighted mean of  $-0.61 \pm 0.42$   $\text{gC}\cdot\text{m}^{-2}\cdot\text{day}^{-1}$  in CMIP6 simulations and  $-0.15 \pm 0.10$   $\text{gC}\cdot\text{m}^{-2}\cdot\text{day}^{-1}$  in observations (Supplementary Table 2). These findings indicate that CMIP6 models realistically simulate VCDs and their adverse impacts on terrestrial carbon uptake around the globe. Observed negative GPP anomalies induced by VCDs are much stronger than anomalies induced by soil droughts or atmospheric aridity alone (Supplementary Fig. 3). The additional effect of soil droughts, i.e., differences in average GPP anomalies between VCDs and atmospheric aridity alone, is greater than the additional effect of atmospheric aridity over 64% of VCD regions, indicating that low SM substantially aggravates the adverse impacts of atmospheric aridity on carbon uptake, especially over mid-latitude dry regions (Supplementary Fig. 3).

SCDs can be identified for every grid cell using the quantile-based approach (Fig. 1b, d). Consistent with previous assessments using CMIP5 models<sup>14</sup>, the quantile-based results from CMIP6 simulations and observations show positive GPP anomalies in high-latitude regions (Fig. 1b, d), where low SM and particularly high VPD tend to enhance terrestrial carbon uptake (Supplementary Fig. 2). In high-latitude regions (north of  $55^\circ\text{N}$ ) where air temperature is low and atmospheric aridity seldom occurs, higher VPD associated with increased temperature promotes photosynthetic carbon uptake and vegetation growth, resulting in a positive correlation between GPP and VPD (see an example in Fig. 1i, j). However, the quantile-based definition of atmospheric aridity does not account for this, and positive average GPP anomalies associated with SCDs are identified over more than 14% of land areas in both observational products and CMIP6 simulations (Fig. 1b, d). This problem is solved by the impact-based approach which accounts for the GPP responses to SM and VPD and can capture the deleterious effect of CDs that lead to negative anomalies of GPP.

The frequency of SCDs (CMIP6:  $2.6 \pm 1.0\%$ ; observations:  $3.5 \pm 1.6\%$ ) is much lower than (only 11% of) that of VCDs (CMIP6:  $24.5 \pm 8.8\%$ ; observations:  $32.0 \pm 11.7\%$ ) (Fig. 2a, b, k, Supplementary Fig. 4a, b and Supplementary Table 2). The higher frequency is induced by higher SM thresholds and lower VPD thresholds for VCDs compared to the 10th percentile SM and 90th percentile VPD for SCDs (Fig. 3a–d and Supplementary Fig. 5). For instance, low SM begins to limit and exert a negative impact on GPP when SM is below the 31st percentile in Grid A located in Amazon Basin and likewise, high VPD begins to adversely affect GPP when VPD above the 74th percentile (Fig. 1e–g). These results indicate a larger number of VCDs that cause negative GPP anomalies over low- and mid-latitude regions, which has been overlooked using a fixed extreme percentile threshold globally. Correspondingly, we find large total GPP anomalies caused by VCDs, with  $-1.44$   $\text{PgC}\cdot\text{yr}^{-1}$  in CMIP6 and  $-0.31$   $\text{PgC}\cdot\text{yr}^{-1}$  in observations at the global scale, while only less than 26% of the total GPP anomalies (CMIP6:  $-0.24$   $\text{PgC}\cdot\text{yr}^{-1}$ ; observations:  $-0.08$   $\text{PgC}\cdot\text{yr}^{-1}$ ) are identified by SCDs (Fig. 2i, j, o, Supplementary Fig. 4i, j and Supplementary Table 2). The large differences in the frequency and total GPP anomalies between the two approaches indicate that the adverse impacts of CDs on land carbon uptake in low- and mid-latitude regions have been considerably underestimated by the widely used quantile-based approach.

In addition to the frequency, we further identify the intensity, duration, and severity of CDs based on the two approaches. CD intensity is measured as the quadratic mean of departures of SM and VPD from their thresholds at the monthly scale, and severity is calculated as the cumulative intensity during consecutive CD months (see “Methods”). Given differences in the thresholds of SM and VPD between the two approaches, the intensity of VCDs is 50% higher than that of SCDs on average, while the duration of the former is 35% longer (Fig. 2c–f, l, m, Supplementary Fig. 4c–f

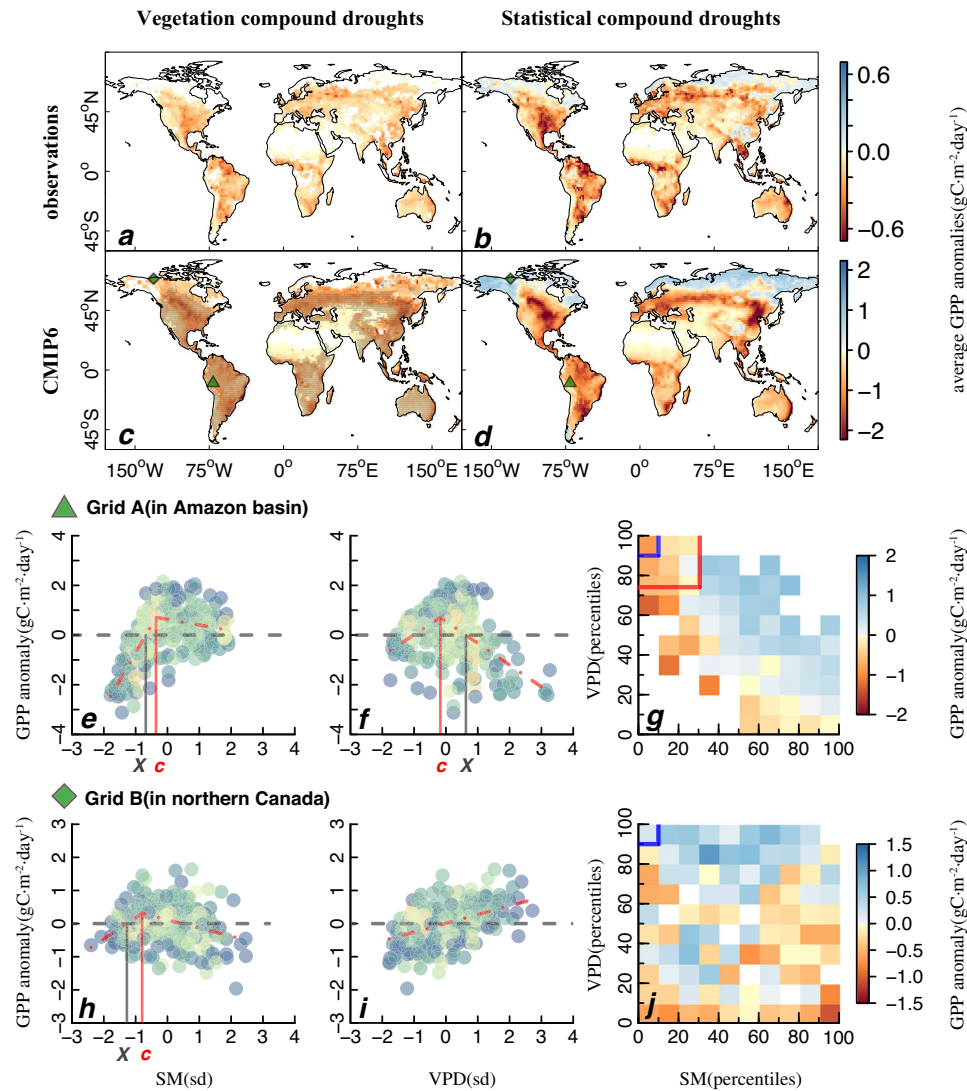


**Fig. 1** Gross primary productivity (GPP) anomaly during vegetation (VCDs) and statistical (SCDs) compound droughts. **a–d** Average GPP anomalies ( $\text{gC}\cdot\text{m}^{-2}\cdot\text{day}^{-1}$ ) for VCDs and SCDs in observations (1981–2017, **a, b**) and CMIP6 historical simulations (1930–2014, **c, d**). Stippling in (**c**) denotes grid cells in which VCDs are detected for at least 7 of 14 models. **e–g** Relationship between GPP anomaly ( $\text{gC}\cdot\text{m}^{-2}\cdot\text{day}^{-1}$ ) and soil moisture (SM) (**e**) or vapor pressure deficit (VPD) (**f**) or both (**g**) for Grid A (▲) located in the Amazon basin (data from MPI-ESM1-2-HR). In scatter plots (**e, f**), the color of the scatters indicates the density of the samples, where higher density in luminous yellow and lower density in pale blue. The red dashed, red solid, and black solid lines represent the fitted response trends, change points, and x-intercepts, respectively. SM and VPD have been standardized by their standard deviation (sd) during the historical period. In the bin plot (**g**), red and blue lines indicate percentile thresholds for VCDs and SCDs, respectively. **h–j** The same as (**e–g**), but for Grid B (◆) located in northern Canada. As GPP always increases with VPD (**i**), VCDs do not occur at Grid B.

and Supplementary Table 2). This suggests that VCDs tend to occur consecutively in the warm season. The combination of higher intensity and extended duration leads to greater severity of VCDs (CMIP6:  $1.30 \pm 0.20$  sd; observations:  $1.42 \pm 0.37$  sd), approximately double that of SCDs (CMIP6:  $0.67 \pm 0.25$  sd; observations:  $0.72 \pm 0.55$  sd) (Fig. 2g, h, n, Supplementary Fig. 4g, h and Supplementary Table 2). Overall, with the impact-based approach, we find more frequent and more severe CD, which lead to larger adverse impacts on terrestrial carbon uptake than previously identified using the quantile-based approach.

### Global hotspots for the occurrence of compound droughts

The global pattern of the frequency of CD identified using the two approaches depends on the thresholds of SM and VPD extremes as well as the correlation of SM and VPD extremes. More frequent SCDs are identified in humid regions, where we also find larger negative

rank correlations between SM and VPD (Fig. 2b and Supplementary Fig. 6). This is consistent with previous studies which suggest that the correlation between dependent variables strongly affects the concurrence frequency of multivariate extremes using the quantile-based approach<sup>17,18</sup>. For example, we find a higher rank correlation ( $r = -0.75$ ) and hence more frequent SCDs in Grid C located in the Amazon Basin than Grid D ( $r = -0.45$ ) located in western Australia (Fig. 3e, h). Additionally, tail dependence of low SM and high VPD may also lead to higher frequency of SCDs (Fig. 3f, i).

Higher frequency of VCDs occurs in regions where GPP is more frequently limited and adversely impacted by high VPD and/or low SM (Fig. 2a and Fig. 3a–d). In other words, if negative anomalies of GPP occur for less extreme low SM and high VPD conditions, a higher frequency of VCDs would be identified, e.g., a higher frequency at Grid D than at Grid C (Fig. 3g, j). In particular, we find a high frequency of VCDs in dryland ecosystems with a

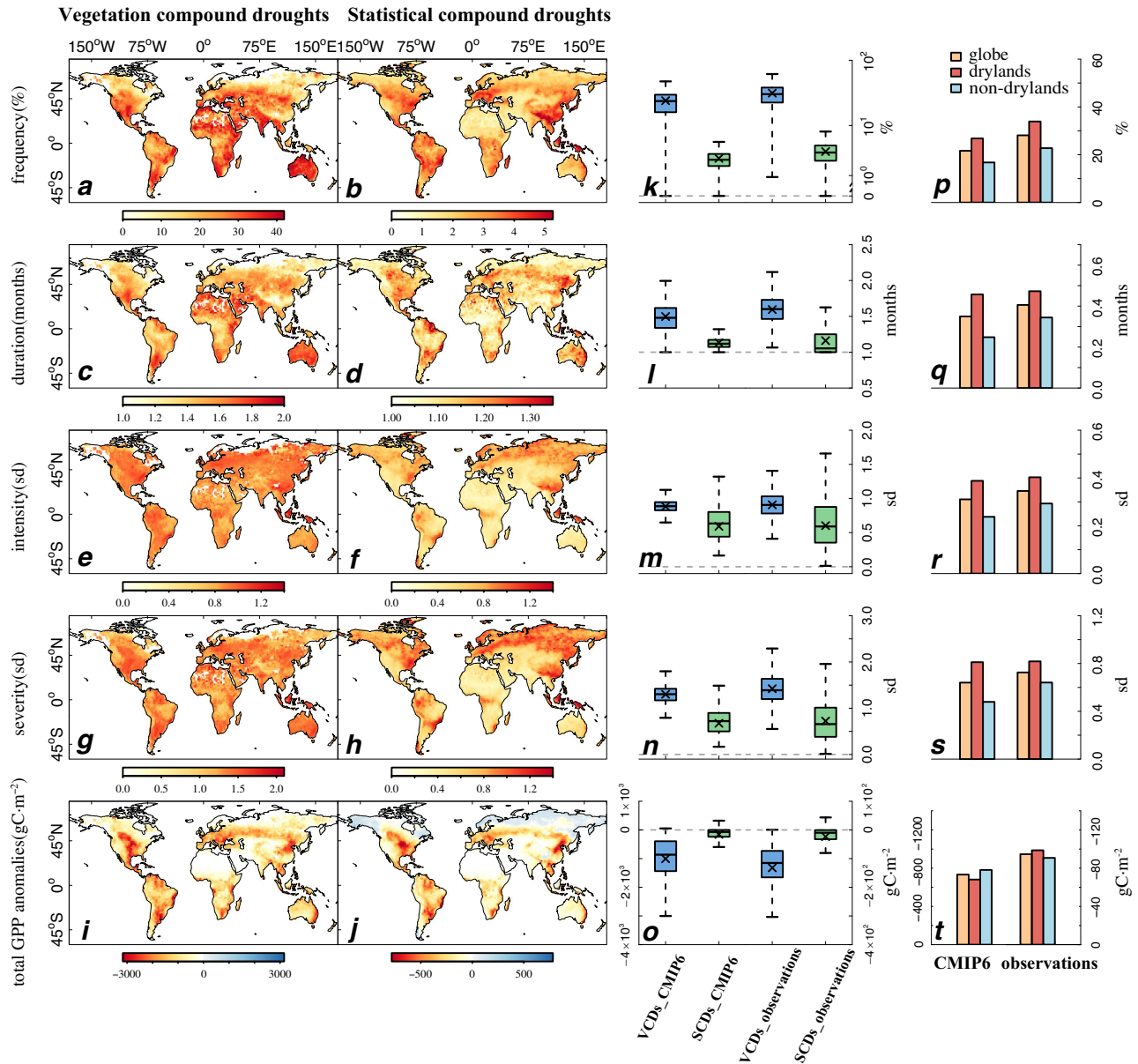


**Fig. 2 Characteristics of vegetation (VCDs) and statistical (SCDs) compound droughts.** **a–j** Spatial distribution of the frequency (% of all warm season months) (**a**, **b**), duration (months) (**c**, **d**), intensity (the departure from thresholds, normalized by the standard deviations of SM and VPD during the historical period, i.e., sd) (**e**, **f**), severity (cumulative intensity for each drought duration, sd) (**g**, **h**), and total GPP anomalies ( $\text{gC}\cdot\text{m}^{-2}$ ) (**i**, **j**) of VCDs and SCDs in CMIP6 historical simulations. **k–o** Boxplots show global frequency, duration, intensity, severity, and total GPP anomalies of VCDs and SCDs in CMIP6 and observations. For each box, middle lines and crosses indicate the median and mean across the globe; the box represents the interquartile range (IQR, the range from 25th to 75th) of the data and whiskers of the box represent the minimum and maximum values of the data, excluding outliers. **p–t** Area-weighted mean of differences in the frequency, duration, intensity, severity, and total GPP anomalies between VCDs and SCDs across the globe, drylands, and non-drylands. The left y-axes in (**o**) and (**t**) apply for CMIP6 and the right ones for observations.

low level of the mean SM and high mean VPD (Supplementary Figs. 7 and 8). In drylands, the negative relationship between SM and VPD caused by land-atmosphere coupling would also increase the frequency of VCDs<sup>37</sup>. Sustained low SM strongly limits evapotranspiration and shifts surface energy partitioning towards sensible heat to increase air temperature, resulting in a warmer and drier atmosphere and a higher VPD<sup>16,17</sup>. At the same time, high VPD enhances evaporative demand to accelerate the drying of the soil. These processes enhance the mutual dependence of SM and VPD, resulting in frequent VCDs and amplified adverse impacts on terrestrial carbon uptake. Such dependence between SM and VPD would be statistically significant when SM falls within

a transitional regime between dry and wet conditions<sup>16,38</sup>. For dryland ecosystems, especially when low SM and high VPD co-occur but are not strongly correlated<sup>38</sup>, it is difficult to detect the dependence of SM and VPD based on correlation and the frequency of VCDs is therefore underestimated using the quantile-based approach.

Compared to non-drylands, we find a larger underestimation of the frequency, duration, intensity, and severity of VCDs in drylands (Fig. 2p–s). This results in a similar magnitude of underestimation of total GPP anomalies between drylands and non-drylands during the historical period, although the mean GPP is much lower in drylands (Fig. 2t). In addition, dryland ecosystems contribute more

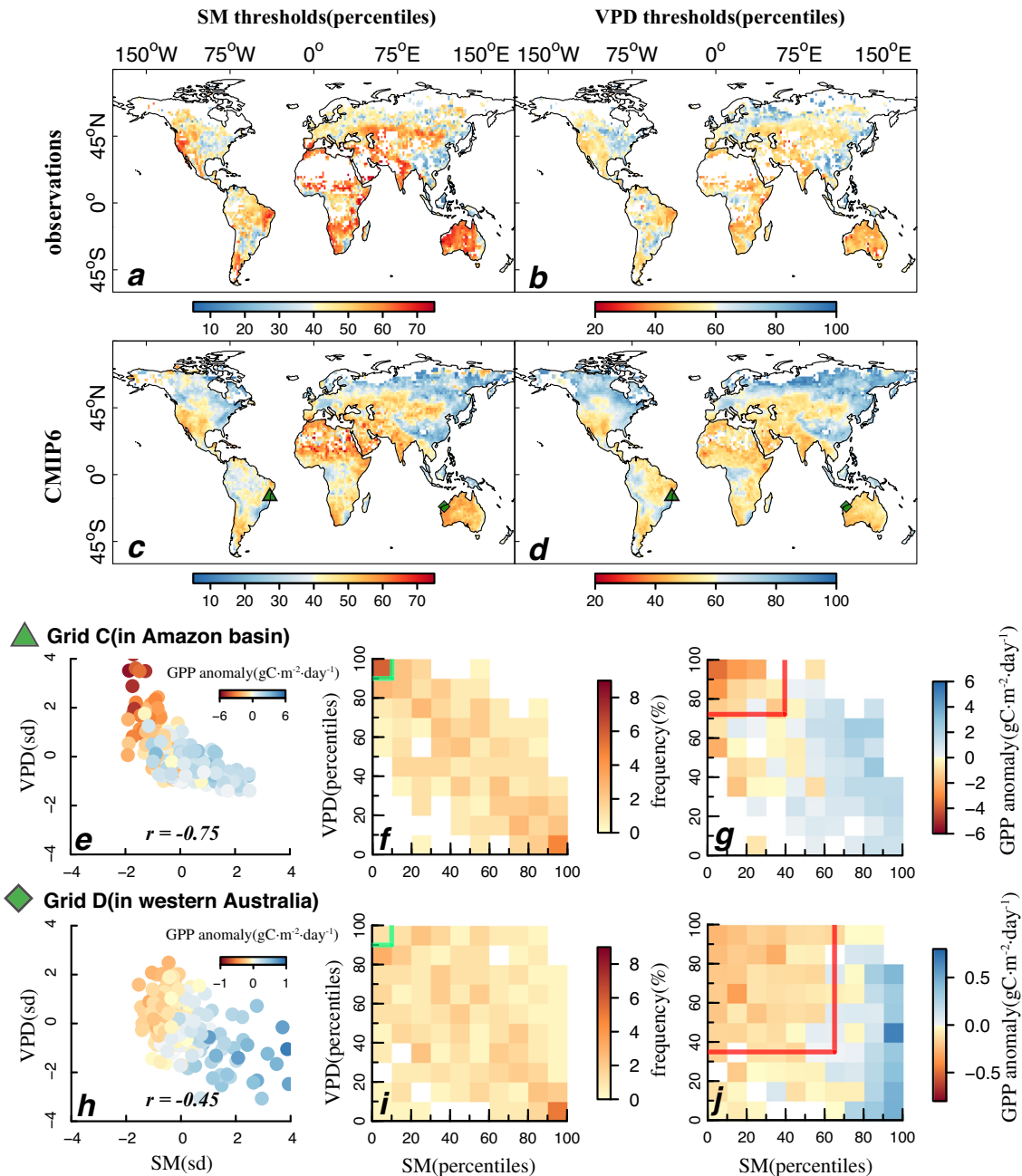


**Fig. 3** SM and VPD thresholds for vegetation compound droughts (VCDs). **a–d** SM and VPD thresholds for VCDs in observations (**a, b**) and CMIP6 (**c, d**) shown as percentile. **e** Relationship between SM and VPD during the warm season for Grid C (▲) located in the Amazon basin (data from CNRM-ESM2-1). The colors in (**e**) denote the GPP anomaly ( $\text{gC}\cdot\text{m}^{-2}\cdot\text{day}^{-1}$ ) and the Spearman (rank) coefficient is shown. SM and VPD have been standardized by their respective standard deviation (sd) during the historical period. **f, g** Frequency (%) and GPP anomaly ( $\text{gC}\cdot\text{m}^{-2}\cdot\text{day}^{-1}$ ) in each percentile bin of SM and VPD. Green and red lines correspond to SM and VPD thresholds for SCDs and VCDs, respectively. **h–j** The same as (**e–g**), but for Grid D (◆) located in western Australia.

than 41% to total GPP anomalies induced by VCDs globally, which corroborates the dominant role of semi-arid systems in the variability of global carbon sink<sup>26,27</sup>. These findings highlight an underestimated risk in terms of the frequency, intensity, severity, and carbon loss of VCDs in drought-prone dryland regions.

### Increases in frequency, intensity, and carbon loss of vegetation compound droughts

To understand future changes in VCDs and their impacts on terrestrial carbon uptake, we use 85-year future simulations

(2016–2100) under the SSP1-2.6 and SSP5-8.5 scenarios compared to the historical simulation (1930–2014). We evaluate the absolute changes in the frequency, intensity, and GPP anomalies of VCDs between the two periods. To facilitate comparison, historical thresholds of SM and VPD extremes are used to define VCDs for the two future scenarios, assuming unchanged vegetation response to drought. In future simulations, we find more frequent VCDs due to climate change over more than 81% of assessed land regions, except in the tropical Africa and South Asia with higher SM (Fig. 4a, b, and Supplementary Fig. 9a, b). Compared to the historical ensemble, the global frequency of VCDs increases by

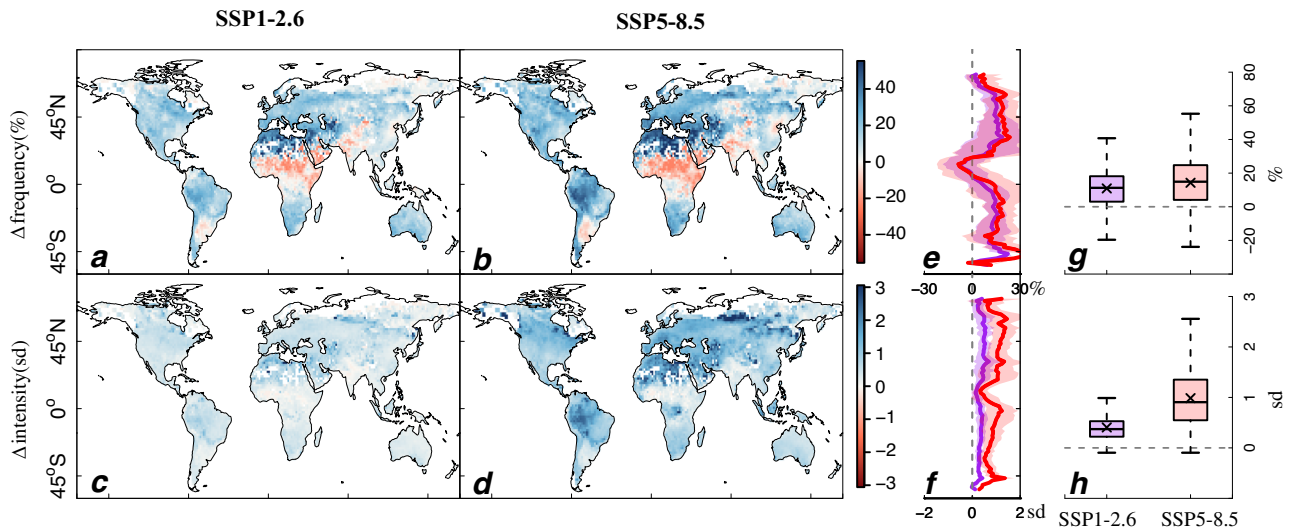


**Fig. 4** Projected changes in the frequency and intensity of vegetation compound droughts (VCDs) in future simulations. **a–d** Future changes in the frequency (%), future minus historical values (**a, b**) and intensity (sd) (**c, d**) of VCDs in SSP1-2.6 and SSP5-8.5 simulations (2016–2100). VCDs in historical and future simulations are defined based on the same thresholds from the historical simulations (1930–2014). **e, f** Latitudinal distribution of changes in the frequency and intensity of VCDs in SSP1-2.6 (purple) and SSP5-8.5 (pink). **g, h** Distribution of changes in the frequency and intensity of VCDs around the globe in SSP1-2.6 and SSP5-8.5 compared to those in the historical simulations. For each box, middle lines and crosses indicate the median and mean across the globe; the box represents the interquartile range (IQR, the range from 25th to 75th) of the data and whiskers of the box represent the minimum and maximum values of the data, excluding outliers.

$10.9 \pm 12.8\%$  in SSP1-2.6 and  $14.3 \pm 16.5\%$  in SSP5-8.5 (Fig. 4g). The increase in the frequency is particularly strong over drying areas where SM declines and VPD rises substantially (Fig. 4a, b, and Supplementary Fig. 9a–d). In addition, we find large increases in the intensity of VCDs in SSP5-8.5 ( $0.99 \pm 0.61$  sd), while the increase in intensity is more than halved ( $0.41 \pm 0.30$  sd) in SSP1-2.6 (Fig. 4f, h). Almost all assessed land areas show greater intensity of VCDs in the future, which is mostly caused by increased VPD, with additional impacts from reduced SM over more than 50% of the land area in SSP1-2.6 and SSP5-8.5 (Fig. 4c, d, and Supplementary Fig. 9a–d). Amazon basin and mid-latitude regions are projected to experience more frequent and more extreme VCDs, particular in SSP5-8.5 (Fig. 4a–d), as these regions are projected to become drier with reduced SM and increased VPD (Supplementary Fig. 9a–d).

The analysis above shows stronger climate change impacts on soil droughts and atmospheric aridity, hence VCDs, without considering potential changes in the GPP responses to SM and VPD in future simulations in which elevated  $\text{CO}_2$  also enhances vegetation growth and carbon uptake and ameliorates the adverse impacts of enhanced water stress<sup>39,40</sup>. To account for this effect, we re-identify future VCDs based on SM and VPD thresholds in each SSP scenario and compare them with historical simulations. There is a small difference in the frequency of VCDs between the future and historical ensembles for both SSP1-2.6 ( $1.6 \pm 4.3\%$ ) and SSP5-8.5 ( $-0.9 \pm 5.5\%$ ) (Fig. 5m). This is because of a higher threshold of VPD and a lower threshold of SM that exert negative impacts on GPP in future simulations (Supplementary Fig. 10). Nevertheless, VCDs are still projected to be more extreme because increased variability of SM and VPD leads to greater departure from future thresholds and an increase in the intensity by 56% in SSP5-8.5 compared to the historical period (Fig. 5n, and Supplementary Fig. 9o, p). Intensification of VCDs poses larger adverse impacts on GPP globally, resulting in increasingly negative GPP anomalies in the future over most regions (Fig. 5e–h), and the total GPP anomalies reduce by  $0.34 \text{ PgC}\cdot\text{yr}^{-1}$  in SSP1-2.6 and  $0.37 \text{ PgC}\cdot\text{yr}^{-1}$  in SSP5-8.5 compared to historical simulations. While the total carbon loss induced by VCDs is similar between SSP1-2.6 and SSP5-8.5, the increases in the intensity and average GPP anomalies in SSP5-8.5 are much greater

compared to those in SSP1-2.6, especially over the Amazon basin and mid-latitude regions that are prone to the climate change impacts (Fig. 5 and Supplementary Fig. 9).

We also identify SCDs based on SM and VPD thresholds in each SSP scenario and find an increased intensity of SCDs and larger negative GPP anomalies over most regions in the future (Supplementary Fig. 11). However, the projected reductions in total GPP anomalies of SCDs are only  $0.05 \text{ PgC}\cdot\text{yr}^{-1}$  in SSP1-2.6 and  $0.01 \text{ PgC}\cdot\text{yr}^{-1}$  in SSP5-8.5 compared to historical simulations, less than 1/6 of the GPP reductions induced by VCDs. This is because the frequency of CDs has been greatly underestimated using the quantile-based approach in historical and future simulations (Fig. 5 and Supplementary Fig. 11). These comparisons indicate that the impact-based approach can better project the frequency of CDs and their adverse impacts on terrestrial carbon uptake in the future.

## DISCUSSION

Our study identifies vegetation compound droughts when low SM and high VPD strongly limit and exert negative impacts on terrestrial carbon uptake. High VPD promotes evaporative demand while low SM limits water supply for plant growth and photosynthetic activities<sup>37</sup>, and concurrent high VPD and low SM exert larger loss of ecosystem carbon uptake than they act in isolation. Given the differences in how GPP responds to low SM and high VPD across biomes and climate zones<sup>36,41</sup>, the thresholds where low SM and high VPD strongly limit and begin to pose negative impacts on GPP vary in space and time. To account for the varying thresholds, the impact-based approach resolves the problem with definition of CDs associated with the widely used quantile-based approach<sup>14,25,42</sup>. Specifically, we show that the frequency of VCDs and associated impacts on terrestrial carbon uptake have been overestimated in high-latitude regions and largely underestimated in low- and mid-latitude regions by the quantile-based approach, which does not consider regional differences in the GPP responses to SM and VPD. This suggests higher risks of CDs to land carbon sink, and associated vegetation growth and food production, than those identified by the

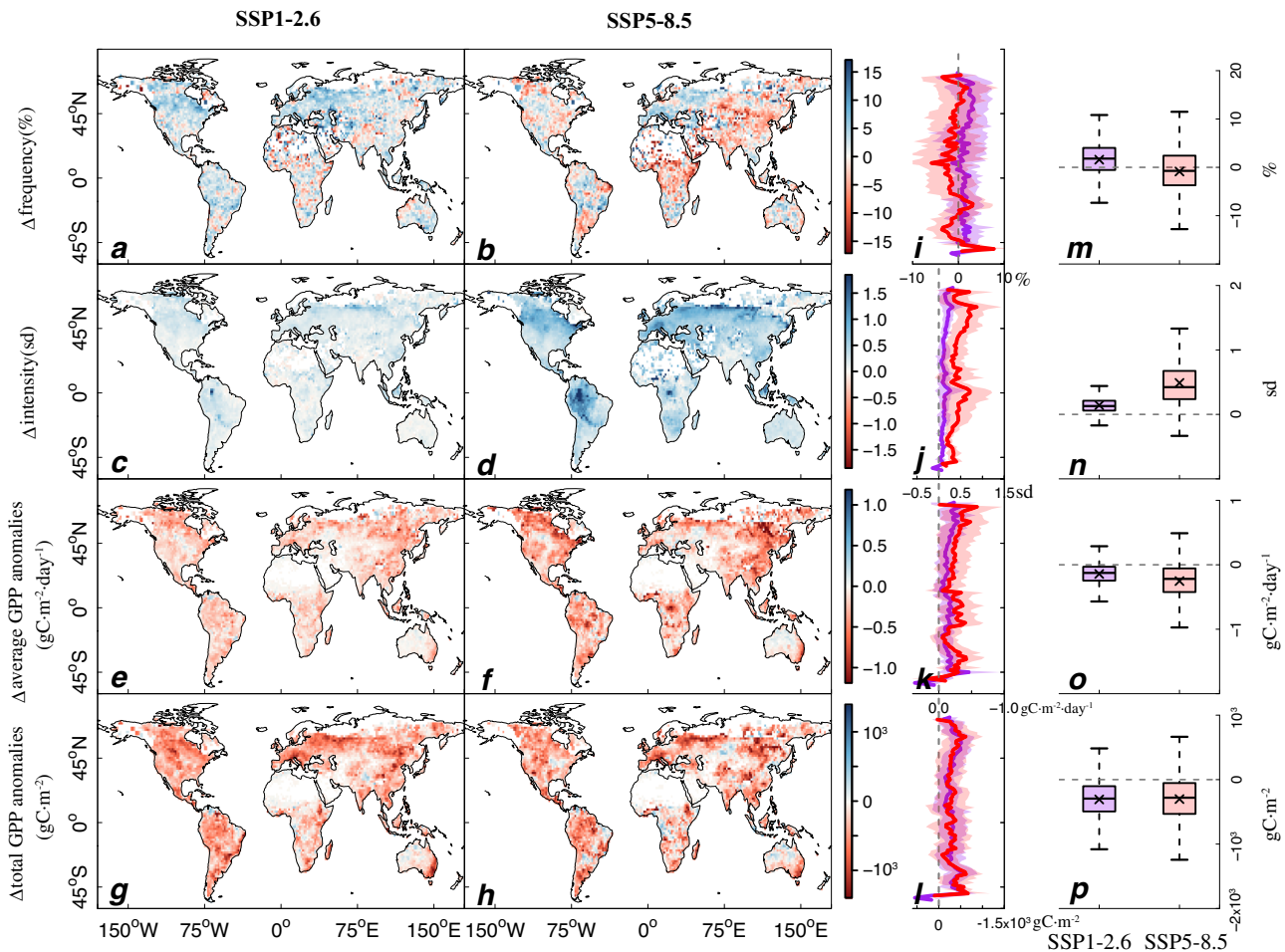


**Fig. 5 Project changes in the frequency, intensity, and GPP anomalies of vegetation compound droughts (VCDs) in future simulations.** **a–h** Future changes in the frequency (%) (**a, b**), intensity (sd) (**c, d**), average GPP anomalies ( $\text{gC}\cdot\text{m}^{-2}\cdot\text{day}^{-1}$ ) (**e, f**), and total GPP anomalies ( $\text{gC}\cdot\text{m}^{-2}$ ) (**g, h**) of VCDs in future simulations. Thresholds used to identify future VCDs are derived from SSP1-2.6 and SSP5-8.5 simulations, respectively. **i–l** Latitudinal distribution of changes in the frequency, intensity, average and total GPP anomalies of VCDs in SSP1-2.6 (purple) and SSP5-8.5 (pink). **m–p** Distribution of changes in the frequency, intensity, average and total GPP anomalies of VCDs around the globe in SSP1-2.6 and SSP5-8.5 compared to those in the historical simulations. For each box, middle lines and crosses indicate the median and mean across the globe; the box represents the interquartile range (IQR, the range from 25th to 75th) of the data and whiskers of the box represent the minimum and maximum values of the data, excluding outliers.

quantile-based approach previously<sup>14</sup>, especially in a warmer climate.

We find a larger underestimation of the frequency, intensity, severity, and GPP anomalies of VCDs in drylands compared to non-drylands. Terrestrial ecosystem carbon uptake in drylands is vulnerable to the adverse impacts of VCDs, which has important implications for understanding the large contribution of dryland ecosystems to the variability of land carbon sink<sup>26,27</sup>. However, the quantile-based approach only identifies the most severe VCDs in drylands with constant thresholds of SM and VPD, but the risk associated with moderate VCDs has largely been ignored. Higher SM thresholds and lower VPD thresholds defined with the impact-based approach suggest a limited capacity of dryland vegetation to deal with water stress and drylands are much more vulnerable to low SM and high VPD, a finding that is consistent with recent studies<sup>33,37</sup>. According to vegetation photosynthesis simulation in most CMIP6 models, this could be explained by the strong coupling of low SM and high VPD and hence aggravated water stress due to strong land-atmosphere interactions<sup>16,37,43</sup>. Recent studies based on in situ measurements also reveal mechanisms related to ecosystem resilience to drought stress. For example, low biodiversity of dryland biomes reduces the resistance of ecosystem productivity to drought, and widespread herbaceous

plants over drylands have insufficient access to deeper soil water<sup>44,45</sup>. Future work is needed to provide a more comprehensive understanding of how water stress impedes carbon uptake via ecosystem structure and functioning, and these process-related parameterizations should be incorporated in Earth system models so that they could better simulate the adverse impacts on terrestrial carbon uptake in dry regions.

VCDs are projected to be more frequent and more severe, causing larger GPP losses in low and particularly high-emission scenarios. Accounting for changes in the GPP responses to SM and VPD leads to little changes in the frequency of VCDs between historical and future simulations. This is because the plant physiological responses to elevated  $\text{CO}_2$ , such as reduced stomatal conductance and transpiration, can conserve water and ameliorate ecohydrological water stress<sup>39,40</sup>. Therefore, plants can maintain the same or even higher rate of photosynthesis at lower SM and higher VPD. However, the projected increases in the intensity of VCDs and resultant stronger carbon loss would greatly limit the capacity of continents to act as a carbon sink in future simulations, especially over the Amazon and mid-latitude regions that are vulnerable to anthropogenic climate change. It is worth noting that recent studies demonstrate that Earth system models generally underestimate the sensitivity of vegetation carbon

uptake to drought stress because models are unable to represent satisfactorily extreme climate events induced by El Niño/Southern Oscillation and other climate drivers<sup>46,47</sup>. In addition, some critical plant hydraulic processes, such as vegetation mortality due to hydraulic failure, are poorly simulated in these models<sup>47,48</sup>. This constitutes a potential source of uncertainty in the projected terrestrial carbon loss induced by VCDs, and the adverse impacts of VCDs on global terrestrial productivity and carbon sink may be greater than those predicted by Earth system models.

Our identification of soil droughts and atmospheric aridity and hence VCDs relies on a general framework of non-monotonical responses of GPP to SM and VPD in warm season months. As tropical rainforest ecosystems can maintain relatively high GPP throughout the year and the growing season differs from the warm season in regions with a Mediterranean climate characterized by wet winters and dry summers, we have repeated our analysis for 3-month growing season with the highest average GPP and all growing months with average GPP larger than 70% of the maximum monthly GPP. The global patterns of the frequency and GPP anomalies of VCDs identified using the impact-based approach are similar for different study periods (Figs. 1, 2 and Supplementary Figs. 12, 13). The global GPP loss in the 3-month warm season ( $-1.44 \text{ PgC}\cdot\text{yr}^{-1}$ ) is larger than the 3-month growing season ( $-1.34 \text{ PgC}\cdot\text{yr}^{-1}$ ), and accounts for 84% of the GPP loss in all growing months ( $-1.72 \text{ PgC}\cdot\text{yr}^{-1}$ ) (Supplementary Table 3). This indicates that GPP reductions caused by VCDs mostly occur in the warm season. We also note an important prerequisite of the impact-based approach is that GPP responds to soil drought or atmospheric aridity concurrently in the same month. The impacts of water stress on vegetation productivity may persist or be present well after a soil drought or atmospheric aridity event is over, the so-called 'drought legacies', which have been demonstrated to be widespread in global ecosystems<sup>49,50</sup>. The legacy effect causes asynchronous drought-driven ecosystem responses, which, however, couldn't be captured by the segmented regression in the study. It is also reported that the legacy effect cannot be accurately detected in Earth system models because of a lack of representation of some fundamental physiological and structural properties of plants<sup>50</sup>. Despite the inherent uncertainties in the models, our analyses combined with observations and state-of-the-art Earth system models have largely resolved the problem in the definition of CDs and provided an improved understanding of spatial and temporal variations in VCDs as well as the adverse impacts on terrestrial carbon cycle.

In summary, our study identifies vegetation compound droughts that have severely limited and exerted adverse impacts on terrestrial carbon uptake and indicates an increased risk of CDs in terms of the frequency, intensity, and adverse impacts on terrestrial carbon uptake due to anthropogenic climate change. Such climate-driven carbon loss through CDs represents a positive feedback loop that may accelerate future climate change and calls for better mitigating strategies, such as reductions in fossil fuels, improved land management practices, and forest restorations, to deal with increased climate risks<sup>51</sup>. More attention should be paid to dryland ecosystems, which have been limited by water stress and are most vulnerable to future intensified CDs. Policymakers and stakeholders should implement effective adaptive measures, such as construction of cross-basin water transfer projects<sup>52</sup>, development of irrigation infrastructures to improve water use efficiency, and cultivation of drought-tolerant crops<sup>9</sup>. These efforts will help improve our capacity to reduce the adverse impacts of climate change in the future and achieve the sustainability of water resources and agricultural production.

## METHODS

### CMIP6 simulations

To evaluate the frequency, intensity, severity of CDs and their impacts on land carbon uptake in past decades and in a warmer future, we used CMIP6 historical simulations (1930–2014) and future projections of two Shared Socioeconomic Pathways (SSPs, 2016–2100): a sustainability scenario SSP1-2.6 with low greenhouse gas (GHG) emissions ( $\text{CO}_2$  emissions cut to net zero around 2075 and radiative forcing reaches  $2.6 \text{ W}\cdot\text{m}^{-2}$  by 2100) and a fossil fuel-intensive scenario with high GHG emissions ( $\text{CO}_2$  emissions triple around 2075 and radiative forcing reaches  $8.5 \text{ W}\cdot\text{m}^{-2}$  by 2100)<sup>53</sup>. We used 14 Earth system models in which monthly total soil moisture content, near-surface air temperature (T), relative humidity (RH), and gross primary productivity (GPP) are available in all three simulations (historical, SSP1-2.6, and SSP5-8.5). VPD was the difference between the saturation and the actual vapor pressure calculated with T and RH. For NorESM2-LM, we used specific humidity, near-surface air pressure, and air temperature to calculate VPD. These models and corresponding ensembles used in this study are shown in Supplementary Table 1.

For each model, we used the grid cells with land fraction higher than 30% for analysis. For each grid cell, we used variables in the warm season, defined as the consecutive 3 months with the highest average temperature during the historical (1930–2014) and future (2016–2100) periods separately. The warm season generally corresponds to the main growing season with the maximum productivity and relatively higher drought stress in temperate and boreal regions. To identify vegetation compound droughts, we first eliminated long-term trends and seasonal cycles of GPP, which may be caused by solar radiation, air temperature, and elevated  $\text{CO}_2$  concentration, by subtracting the 30-year centered running mean from GPP for the corresponding month during the historical and future periods to calculate the GPP anomalies for each month. We further identified the soil droughts and atmospheric aridity based on the impacts of SM and VPD on monthly GPP anomalies, which can largely eliminate the impacts of other influencing factors (see "Identification of vegetation compound droughts" below).

### Observational datasets

To identify CDs, we also used root-zone SM from the Global Land Evaporation Amsterdam Model (GLEAM) v3.5a, which covers the period of 1980–2020 with a spatial resolution of  $0.25^\circ \times 0.25^\circ$ . GLEAM is a semi-empirical model for estimating potential/actual evapotranspiration, interception loss, snow sublimation, and soil moisture<sup>54</sup>, constrained by satellite and reanalysis data and has been widely used in climate, hydrological, and ecological research<sup>28</sup>. To improve the accuracy of SM estimates, two microwave-based SM observations and surface SM from the Noah model are assimilated into GLEAM by Newtonian nudging algorithm<sup>28</sup>. The SM product has been successfully validated under different vegetation and climate conditions in comparison with in situ measurements at 30 sites of Soil Climate Analysis Network and 2325 soil moisture sensors from International Soil Moisture Network<sup>28,54</sup>.

We calculated VPD from near-surface air temperature and dew-point temperature (i.e., the temperature to which air needs to be cooled at constant pressure to achieve saturation) from Modern-Era Retrospective analysis for Research and Applications, Version 2 (MERRA-2) at the spatial resolution of  $1^\circ \times 1^\circ$ . MERRA-2 provides an ongoing near-real-time climate analysis since 1980 with improvements in quality compared to MERRA. The improvements include bias reduction to ensure mass balance for a number of atmospheric and hydrological variables<sup>29</sup>. The air temperature and humidity were largely determined from direct assimilation of satellite measurements of irradiance<sup>55</sup>.



We used monthly GPP outputs at  $0.5^\circ \times 0.5^\circ$  from the FLUXCOM dataset. FLUXCOM used three machine learning algorithms (random forest, artificial neural network, and multivariate adaptive regression splines) to upscale carbon flux measurements from 224 eddy covariance towers to produce global gridded GPP along with satellite and meteorological data<sup>30</sup>. GPP was estimated as the median value generated by the three algorithms for each grid cell. The cross-consistency checks of FLUXCOM GPP with GPP from sun-induced fluorescence and dynamic global vegetation models have demonstrated the high quality of FLUXCOM in generating its spatial patterns and temporal variations<sup>30</sup>. We selected two ensembles from ERA-5 and CRU JRA v1.1 meteorological forcing data separately because they cover the period of 1981–2017, and the satellite datasets from Moderate Resolution Imaging Spectroradiometer (MODIS).

Consistent with model simulations, we extracted SM, VPD, and GPP of the warm season over the 1981–2017 period and subtracted 30-year centered running mean from monthly GPP to eliminate long-term trends and seasonal cycles and obtain GPP anomalies. To allow for a fair comparison, data analyses of observational datasets and multi-model simulations were bilinearly interpolated to a common spatial resolution of  $1.5^\circ \times 1.5^\circ$  to obtain the ensemble results.

### Drylands

The extent of global drylands is based on the United Nations Convention to Combat Desertification (UNCCD) definition, covering 46% of the land area excluding Antarctica and Greenland (Supplementary Fig. 7). Drylands include hyper-arid, arid, semi-arid, and dry sub-humid areas, with the aridity index, i.e., the ratio of precipitation over the potential evapotranspiration, less than 0.65. The aridity index is calculated using climate data from the global climate dataset produced by the Climate Research Unit of the University of East Anglia, UK<sup>56</sup>.

### Identification of vegetation compound droughts

A two-segment linear regression model provides a first-order representation of the GPP responses to SM and VPD. A significant break in the slope would indicate that there is a change-point for SM or VPD above which GPP would respond to SM or VPD differently (Supplementary Fig. 1)<sup>31,57</sup>. The fitted two-segment regression (SEG) for a grid cell can be expressed as:

$$Y = \begin{cases} \alpha_0 + \beta_0 X + \varepsilon, & X < c \\ \alpha_1 + \beta_1 X + \varepsilon, & X > c \end{cases} \quad (1)$$

where  $Y$  is the GPP anomaly in  $\text{gC}\cdot\text{m}^{-2}\cdot\text{day}^{-1}$ ,  $X$  represents SM or VPD,  $c$  the change-point for SM or VPD, and  $\varepsilon$  the error term. Parameters ( $\alpha_0$ ,  $\alpha_1$ ,  $\beta_0$ , and  $\beta_1$ ) can be estimated through the ordinary least squares, and  $c$  estimated with a grid search method together with bootstrap<sup>57</sup>. To ensure continuity of GPP anomalies at the change-point  $c$ , we forced GPP anomaly to be identical at  $c$ , i.e.,  $\alpha_0 + \beta_0 c = \alpha_1 + \beta_1 c$ .

We further tested the significance of the change in slope with bootstrapping. Null ( $H_0$ ) and alternative ( $H_a$ ) hypotheses of the test are:

$$H_0: \beta_0 = \beta_1; H_a: \beta_0 \neq \beta_1 \quad (2)$$

When the difference in the slope is significant, the segmented linear equations can be used to characterize the change in how the GPP anomaly responds to SM and VPD, otherwise Eq. 1 is degenerated into a univariate linear (UL) regression equation:

$$Y = \alpha_2 + \beta_2 X + \varepsilon \quad (3)$$

According to our understanding of how GPP responds to SM and VPD (Supplementary Fig. 1), vegetation carbon uptake is strongly limited by water availability when SM is below and VPD is

above the change-point. Under the drought-limited regime, GPP increases with SM and decreases with VPD<sup>32,37</sup>. To capture this regime, the regression coefficients for the drought-limited phase,  $\beta_0$  or  $\beta_2$ , should be significantly positive for SM and,  $\beta_1$  or  $\beta_2$ , significantly negative for VPD. Cases meeting this criterion are shown in Supplementary Fig. 14. In order to characterize the adverse impacts of soil droughts and atmospheric aridity on GPP, we compared the change-point for the cases SEG01 and SEG02 in Supplementary Fig. 14 with the x-intercept at which the regression line crosses the x-axis (zero GPP anomaly) and chose the lower value as the SM threshold and the higher value as the VPD threshold. Therefore, the x-intercept was taken as the threshold for SEG01, while the change-point was taken for SEG02. For the case UL, the x-intercept was directly taken because the change-point does not exist based on the univariate linear regression.

There are two exceptional cases in the identification (EXP01 and EXP02). (i) Drought-limited phase is too weak (EXP01): specifically, GPP anomaly always remains above zero in the drought-limited phase because the limitation of low SM (high VPD) is too weak to cause adverse impacts. Hence, soil droughts or atmospheric aridity were not identified for this case. (ii) Permanent drought-limited (EXP02): as SM decreases, GPP anomaly declines rapidly when SM is above the change-point and gradually when SM falls below the change-point. Likewise, as VPD rises, GPP declines more rapidly when VPD is below the change-point and gradually when VPD is above the change-point. This case occurs in dry and hyper-dry regimes in Supplementary Fig. 1. SM/VPD thresholds always equal the x-intercept regardless of change-point because vegetation productivity has already been strongly reduced by low SM and high VPD under the dry regime.

This procedure was performed for each grid cell during historical and future periods. Segmented regression and x-intercept solving were implemented in R 4.1.2 using 'chngpt' and 'rootSolve' packages separately<sup>57,58</sup>.

Fitted regressions are dominated by SEG01 and UL over 75% of assessed land area in CMIP6 historical simulations and observations (Supplementary Fig. 15). As expected, UL captures the relationship between GPP and SM or VPD for dry regimes and is identified mainly in drylands. SEG01 describes the impacts of SM and VPD on GPP from dry to wet regimes and is found in humid areas in the tropics and high-latitude regions (Supplementary Fig. 15i, j). The spatial distribution of the fitted regression cases therefore supports the conceptual framework shown in Supplementary Fig. 1.

We identified the thresholds at which low SM and high VPD strongly limit and exert adverse impacts on GPP using the fitted regression of GPP response to SM and VPD for each grid cell. VCDs were defined as months with SM below its threshold and VPD above its threshold simultaneously in observations and CMIP6 historical simulations (Fig. 1). To project future changes in VCDs and their adverse impacts on terrestrial carbon uptake, we defined VCDs in SSP1-2.6 and SSP5-8.5 based on (i) the same thresholds from historical simulations to determine the impacts of climate change on SM and VPD and hence VCDs (Fig. 4), and (ii) separate thresholds from each of future scenarios to account for the impacts of future climate change and elevated  $\text{CO}_2$  on potential changes in the GPP responses to SM and VPD, which is essential to assess the GPP anomalies induced by VCDs in the future (Fig. 5). We also compared the thresholds from future scenarios with those from historical simulations, and lower SM and higher VPD thresholds indicate that elevated  $\text{CO}_2$  may have ameliorated ecohydrological water stress (Supplementary Fig. 10).

### Characteristics of compound droughts

We analyzed the frequency, duration, intensity, and severity of CDs and associated average and total GPP anomalies. Average and

total GPP anomalies are the mean and sum of GPP anomalies during CD months, respectively. Frequency is calculated as the proportion of CD months in warm season months (255 months over 85 years in total for the historical or future simulations and 111 months over 37 years for observations). Duration is the mean length of months that CDs last in the warm season, and intensity is the quadratic mean of departures of SM and VPD from their thresholds for CDs. To facilitate comparison, we used the standard deviations of SM and VPD during the historical period to normalize the departures, and the intensity is expressed as:

$$Intensity = \sum_{i=1}^{N_m} \frac{\sqrt{\left[\frac{SM_i - SM_t}{\sigma(SM)}\right]^2 + \left[\frac{VPD_i - VPD_t}{\sigma(VPD)}\right]^2}}{\sqrt{2}N_m} \quad (4)$$

where  $N_m$  is the number of CD months,  $\sigma(SM)$  and  $\sigma(VPD)$  are standard deviations of SM and VPD, respectively, in observations/historical simulations.  $SM_t$  and  $VPD_t$  are the thresholds of SM and VPD extremes, respectively.

As the severity of a drought/aridity event depends on its intensity and duration, it is calculated as the summed intensity over consecutive CD months in each warm season:

$$Sev\_SM = \sum_{k=1}^D \frac{|SM_k - SM_t|}{\sigma(SM)} \quad (5)$$

$$Sev\_VPD = \sum_{k=1}^D \frac{|VPD_k - VPD_t|}{\sigma(VPD)} \quad (6)$$

where  $D$  is the number of months, i.e., the duration of CDs, ranging from 1 to 3 in a warm season.  $SM_k$  and  $VPD_k$  are the SM and VPD in the  $k$ th drought/aridity month.  $Sev\_SM$  and  $Sev\_VPD$  are measures of severity of a consecutive soil drought or atmospheric aridity event, respectively. The severity of CDs is calculated as the quadratic mean of this severity measure for soil drought and atmospheric aridity events:

$$Severity = \sum_{j=1}^{N_D} \frac{\sqrt{Sev\_SM_j^2 + Sev\_VPD_j^2}}{\sqrt{2}N_D} \quad (7)$$

where  $N_D$  is the number of consecutive CD events that range from 1 to 3 months in all warm seasons.

For data analyses, we calculated the frequency, duration, intensity, severity, and GPP anomalies of VCDs, which were compared with the characteristics of SCDs in observations and CMIP6 simulations. We also assessed future changes in the frequency, intensity, and GPP anomalies of VCDs and SCDs in SSP1-2.6 and SSP5-8.5 relative to historical simulations.

### Uncertainty in the identification of vegetation compound droughts

The identification of VCDs using the impact-based approach may depend on how the growing season for GPP is defined. Although the 3 warmest months used in the main text typically correspond to the main growing season in mid- and high-latitude regions, it is probably not the case in tropical regions. Given that tropical rainforest ecosystems could maintain high GPP all year round instead of just during the 3-month warm season, there may be substantial GPP losses due to VCDs in other seasons. To further confirm the effectiveness of the impact-based approach, we evaluated GPP anomalies using all months for the growth season (Supplementary Fig. 13) and the 3-month growing season with the highest average GPP (Supplementary Fig. 12), in addition to the 3 warmest months. A growing month is defined as a month with the average GPP exceeding 70% of the maximum monthly GPP (Supplementary Fig. 13). We compared global total GPP anomalies identified using the impact-based approach in the 3 warmest

months and all growing months to test whether the adverse impacts of VCDs on terrestrial carbon uptake mostly occur in the warm season (Supplementary Table 3).

### DATA AVAILABILITY

Datasets used in this study are available online. The CMIP6 simulations were downloaded from <https://esgf-node.llnl.gov/search/CMIP6/>. The GLEAMv3.5a are available from <https://www.gleam.eu/#downloads>, the MERRA-2 reanalysis data from <https://disc.gsfc.nasa.gov/datasets?project=MERRA-2>, and the FLUXCOM dataset from <https://www.bgc-jena.mpg.de/geodb/projects/Home.php>. The dryland area is available from <https://landportal.org/book/dataset/unep-wcmm-dry>.

### CODE AVAILABILITY

The R scripts used for data analyses are available upon reasonable request.

Received: 11 September 2023; Accepted: 8 January 2024;

Published online: 19 January 2024

### REFERENCES

- IPCC. *Climate Change 2021: The Physical Science Basis. Contribution of Working Group I to the Sixth Assessment Report of the Intergovernmental Panel on Climate Change* (eds Masson-Delmotte, V. et al.). (Cambridge University Press, 2021).
- Zhou, S., Yu, B. & Zhang, Y. Global concurrent climate extremes exacerbated by anthropogenic climate change. *Sci. Adv.* **9**, eabo1638 (2023).
- Cook, B. I. et al. Twenty-first century drought projections in the CMIP6 forcing scenarios. *Earths Future* **8**, e2019EF001461 (2020).
- Hao, Z. et al. Compound droughts and hot extremes: characteristics, drivers, changes, and impacts. *Earth-Sci. Rev.* **235**, 104241 (2022).
- Yin, J. et al. Future socio-ecosystem productivity threatened by compound drought heatwave events. *Nat. Sustain.* **6**, 259–272 (2023).
- Novick, K. A. et al. The increasing importance of atmospheric demand for ecosystem water and carbon fluxes. *Nat. Clim. Change* **6**, 1023–1027 (2016).
- Fu, Z. et al. Atmospheric dryness reduces photosynthesis along a large range of soil water deficits. *Nat. Commun.* **13**, 989 (2022).
- Madadgar, S., AghaKouchak, A., Farahmand, A. & Davis, S. J. Probabilistic estimates of drought impacts on agricultural production. *Geophys. Res. Lett.* **44**, 7799–7807 (2017).
- Ciais, P. et al. Europe-wide reduction in primary productivity caused by the heat and drought in 2003. *Nature* **437**, 529–533 (2005).
- McDowell, N. et al. Mechanisms of plant survival and mortality during drought: why do some plants survive while others succumb to drought? *N. Phytol.* **178**, 719–739 (2008).
- Peng, C. et al. A drought-induced pervasive increase in tree mortality across Canada's boreal forests. *Nat. Clim. Change* **1**, 467–471 (2011).
- Chaves, M. M., Flexas, J. & Pinheiro, C. Photosynthesis under drought and salt stress: regulation mechanisms from whole plant to cell. *Ann. Bot.* **103**, 551–560 (2009).
- Zhang, Y. et al. Canopy and physiological controls of GPP during drought and heat wave. *Geophys. Res. Lett.* **43**, 3325–3333 (2016).
- Zhou, S., Zhang, Y., Park Williams, A. & Gentile, P. Projected increases in intensity, frequency, and terrestrial carbon costs of compound drought and aridity events. *Sci. Adv.* **5**, eaau5740 (2019).
- Dannenberg, M. P. et al. Exceptional heat and atmospheric dryness amplified losses of primary production during the 2020 U.S. Southwest hot drought. *Glob. Change Biol.* **28**, 4797–4806 (2022).
- Seneviratne, S. I. et al. Investigating soil moisture–climate interactions in a changing climate: a review. *Earth Sci. Rev.* **99**, 125–161 (2010).
- Zhou, S. et al. Land–atmosphere feedbacks exacerbate concurrent soil drought and atmospheric aridity. *Proc. Natl Acad. Sci. USA* **116**, 18848–18853 (2019).
- Zscheischler, J. & Seneviratne, S. I. Dependence of drivers affects risks associated with compound events. *Sci. Adv.* **3**, e1700263 (2017).
- Leonard, M. et al. A compound event framework for understanding extreme impacts. *WIREs Clim. Change* **5**, 113–128 (2014).
- Zscheischler, J. et al. Future climate risk from compound events. *Nat. Clim. Change* **8**, 469–477 (2018).
- Wang, H., Wang, R., Harrison, S. P. & Prentice, I. C. Leaf morphological traits as adaptations to multiple climate gradients. *J. Ecol.* **110**, 1344–1355 (2022).
- Hanan, N. P., Milne, E., Aynekulu, E., Yu, Q. & Anchang, J. A role for drylands in a carbon neutral world? *Front. Environ. Sci.* **9**, 786087 (2021).

23. Caferra, R. & Bassi, R. Plants and water in a changing world: a physiological and ecological perspective. *Rend. Lincei Sci. Fis. E Nat.* **33**, 479–487 (2022).
24. Nemani, R. R. et al. Climate-driven increases in global terrestrial net primary production from 1982 to 1999. *Science* **300**, 1560–1563 (2003).
25. Reichstein, M. et al. Climate extremes and the carbon cycle. *Nature* **500**, 287–295 (2013).
26. Ahlström, A. et al. The dominant role of semi-arid ecosystems in the trend and variability of the land CO<sub>2</sub> sink. *Science* **348**, 895–899 (2015).
27. Huang, L. et al. Drought dominates the interannual variability in global terrestrial net primary production by controlling semi-arid ecosystems. *Sci. Rep.* **6**, 24639 (2016).
28. Martens, B. et al. GLEAM v3: satellite-based land evaporation and root-zone soil moisture. *Geosci. Model Dev.* **10**, 1903–1925 (2017).
29. Gelaro, R. et al. The modern-era retrospective analysis for research and applications, version 2 (MERRA-2). *J. Clim.* **30**, 5419–5454 (2017).
30. Jung, M. et al. Scaling carbon fluxes from eddy covariance sites to globe: synthesis and evaluation of the FLUXCOM approach. *Biogeosciences* **17**, 1343–1365 (2020).
31. Berdugo, M. et al. Global ecosystem thresholds driven by aridity. *Science* **367**, 787–790 (2020).
32. Rogers, A. et al. A roadmap for improving the representation of photosynthesis in Earth system models. *N. Phytol.* **213**, 22–42 (2017).
33. Li, X. et al. Global variations in critical drought thresholds that impact vegetation. *Natl Sci. Rev.* **10**, nwad049 (2023).
34. Green, J. K. et al. Large influence of soil moisture on long-term terrestrial carbon uptake. *Nature* **565**, 476–479 (2019).
35. Li, Y., Guan, K., Schnitkey, G. D., DeLucia, E. & Peng, B. Excessive rainfall leads to maize yield loss of a comparable magnitude to extreme drought in the United States. *Glob. Change Biol.* **25**, 2325–2337 (2019).
36. Wang, H. et al. Exploring complex water stress–gross primary production relationships: Impact of climatic drivers, main effects, and interactive effects. *Glob. Change Biol.* **28**, 4110–4123 (2022).
37. Fu, Z. et al. Critical soil moisture thresholds of plant water stress in terrestrial ecosystems. *Sci. Adv.* **8**, eabq7827 (2022).
38. Hsu, H. & Dirmeyer, P. A. Soil moisture–evaporation coupling shifts into new gears under increasing CO<sub>2</sub>. *Nat. Commun.* **14**, 1162 (2023).
39. Lian, X. et al. Multifaceted characteristics of dryland aridity changes in a warming world. *Nat. Rev. Earth Environ.* **2**, 232–250 (2021).
40. Cheng, L. et al. Recent increases in terrestrial carbon uptake at little cost to the water cycle. *Nat. Commun.* **8**, 110 (2017).
41. Stocker, B. D. et al. Quantifying soil moisture impacts on light use efficiency across biomes. *N. Phytol.* **218**, 1430–1449 (2018).
42. Wu, X. & Jiang, D. Probabilistic impacts of compound dry and hot events on global gross primary production. *Environ. Res. Lett.* **17**, 034049 (2022).
43. Humphrey, V. et al. Soil moisture–atmosphere feedback dominates land carbon uptake variability. *Nature* **592**, 65–69 (2021).
44. Hoover, D. L., Duniway, M. C. & Belnap, J. Testing the apparent resistance of three dominant plants to chronic drought on the Colorado Plateau. *J. Ecol.* **105**, 152–162 (2017).
45. Liu, D., Wang, T., Peñuelas, J. & Piao, S. Drought resistance enhanced by tree species diversity in global forests. *Nat. Geosci.* **15**, 800–804 (2022).
46. Timmermann, A. et al. El Niño–Southern Oscillation complexity. *Nature* **559**, 535–545 (2018).
47. Liu, L. et al. Increasingly negative tropical water–interannual CO<sub>2</sub> growth rate coupling. *Nature* **618**, 755–760 (2023).
48. Li, W. et al. Widespread increasing vegetation sensitivity to soil moisture. *Nat. Commun.* **13**, 3959 (2022).
49. Müller, L. M. & Bahn, M. Drought legacies and ecosystem responses to subsequent drought. *Glob. Change Biol.* **28**, 5086–5103 (2022).
50. Anderegg, W. R. L. et al. Pervasive drought legacies in forest ecosystems and their implications for carbon cycle models. *Science* **349**, 528–532 (2015).
51. IPCC. *Climate Change 2022: Mitigation of Climate Change. Contribution of Working Group III to the Sixth Assessment Report of the Intergovernmental Panel on Climate Change* (eds Shukla, P. R. et al.) (Cambridge University Press, 2022).
52. Liu, J. & Yang, W. Water sustainability for China and beyond. *Science* **337**, 649–650 (2012).
53. O'Neill, B. C. et al. The scenario model intercomparison project (ScenarioMIP) for CMIP6. *Geosci. Model Dev.* **9**, 3461–3482 (2016).
54. Miralles, D. G. et al. Global land-surface evaporation estimated from satellite-based observations. *Hydrol. Earth Syst. Sci.* **15**, 453–469 (2011).
55. Will, M. et al. MERRA-2 input observations: summary and assessment. in *Technical Report Series on Global Modeling and Data Assimilation* Vol. 46, 8–12 (2016).
56. Levke, S. A *Spatial Analysis Approach to the Global Delineation of Dryland Areas of Relevance to the CBD Programme of Work on Dry and Subhumid Lands*. <https://docslib.org/doc/2573884/a-spatial-analysis-approach-to-the-global-delineation-of-dryland-areas-of-relevance-to-the-cbd-programme-of-work-on-dry-and-subhumid-lands> (2007).
57. Fong, Y., Huang, Y., Gilbert, P. B. & Permar, S. R. chngpt: threshold regression model estimation and inference. *BMC Bioinform.* **18**, 454 (2017).
58. Soetaert, K. & Herman, P. M. A *Practical Guide to Ecological Modelling. Using R as a Simulation Platform* (Springer, 2009).

## ACKNOWLEDGEMENTS

We acknowledge the World Climate Research Programme's Working Group on Coupled Modelling, which is responsible for CMIP, and we thank the climate modeling groups (listed in Supplementary Table 1 of this paper) for producing and making available their model output. For CMIP, the U.S. Department of Energy's Program for Climate Model Diagnosis and Intercomparison provides coordinating support and led development of software infrastructure in partnership with the Global Organization for Earth System Science Portals. This work was supported by the National Natural Science Foundation of China (41991235), the National Key Research and Development Program of China (2022YFF0801300), the NSFC Excellent Young Scientists Fund (Overseas) and the Fundamental Research Funds for the Central Universities. We thank the high-performance computing support from the Center for Geodata and Analysis, Faculty of Geographical Science, Beijing Normal University (<https://gda.bnu.edu.cn/>).

## AUTHOR CONTRIBUTIONS

S.Z. conceived and designed the study. J.S. processed model simulations and reanalysis data. S.Z. and J.S. interpreted the results and led the manuscript writing. All authors edited and revised the manuscript.

## COMPETING INTERESTS

The authors declare no competing interests.

## ADDITIONAL INFORMATION

**Supplementary information** The online version contains supplementary material available at <https://doi.org/10.1038/s41612-024-00571-y>.

**Correspondence** and requests for materials should be addressed to Sha Zhou.

**Reprints and permission information** is available at <http://www.nature.com/reprints>

**Publisher's note** Springer Nature remains neutral with regard to jurisdictional claims in published maps and institutional affiliations.



**Open Access** This article is licensed under a Creative Commons Attribution 4.0 International License, which permits use, sharing, adaptation, distribution and reproduction in any medium or format, as long as you give appropriate credit to the original author(s) and the source, provide a link to the Creative Commons license, and indicate if changes were made. The images or other third party material in this article are included in the article's Creative Commons license, unless indicated otherwise in a credit line to the material. If material is not included in the article's Creative Commons license and your intended use is not permitted by statutory regulation or exceeds the permitted use, you will need to obtain permission directly from the copyright holder. To view a copy of this license, visit <http://creativecommons.org/licenses/by/4.0/>.

© The Author(s) 2024